

High-performance continuous-wave operation of superlattice terahertz quantum-cascade lasers

Cite as: Appl. Phys. Lett. **82**, 1518 (2003); <https://doi.org/10.1063/1.1559419>

Submitted: 01 November 2002 • Accepted: 08 January 2003 • Published Online: 04 March 2003

Rüdeger Köhler, Alessandro Tredicucci, Fabio Beltram, et al.



View Online



Export Citation

ARTICLES YOU MAY BE INTERESTED IN

Thermoelectrically cooled THz quantum cascade laser operating up to 210 K


Applied Physics Letters **115**, 010601 (2019); <https://doi.org/10.1063/1.5110305>

Far-infrared ($\lambda=87\ \mu\text{m}$) bound-to-continuum quantum-cascade lasers operating up to 90 K


Applied Physics Letters **82**, 3165 (2003); <https://doi.org/10.1063/1.1571653>

High-power terahertz quantum cascade lasers with $\sim 0.23\ \text{W}$ in continuous wave mode

AIP Advances **6**, 075210 (2016); <https://doi.org/10.1063/1.4959195>



HIDEN
ANALYTICAL




Instruments for Advanced Science

- Knowledge,
- Experience,
- Expertise

Click to view our product catalogue


Contact Hiden Analytical for further details:
www.HidenAnalytical.com
info@hideninc.com

Gas Analysis




- ▶ dynamic measurement of reaction gas streams
- ▶ catalysis and thermal analysis
- ▶ molecular beam studies
- ▶ dissolved species probes
- ▶ fermentation, environmental and ecological studies

Surface Science




- ▶ UHVTPD
- ▶ SIMS
- ▶ end point detection in ion beam etch
- ▶ elemental imaging - surface mapping

Plasma Diagnostics



- ▶ plasma source characterization
- ▶ etch and deposition process reaction kinetic studies
- ▶ analysis of neutral and radical species

Vacuum Analysis



- ▶ partial pressure measurement and control of process gases
- ▶ reactive sputter process control
- ▶ vacuum diagnostics
- ▶ vacuum coating process monitoring

High-performance continuous-wave operation of superlattice terahertz quantum-cascade lasers

Rüdeger Köhler,^{a)} Alessandro Tredicucci, and Fabio Beltram
NEST-INFM and Scuola Normale Superiore, Piazza dei Cavalieri 7, 56126 Pisa, Italy

Harvey E. Beere, Edmund H. Linfield, A. Giles Davies, and David A. Ritchie
Cavendish Laboratory, University of Cambridge, Madingley Road CB3 0HE, Cambridge, United Kingdom

Sukhdeep S. Dhillon and Carlo Sirtori
Thales Research & Technology, Domaine de Corbeville, 91404 Orsay, France

(Received 1 November 2002; accepted 8 January 2003)

The cw operation of chirped-superlattice quantum-cascade lasers emitting at $\lambda \sim 67 \mu\text{m}$ (4.4 THz) is analyzed. Collected (min. 33% efficiency) output powers of 4 mW per facet are measured at liquid helium temperatures and a maximum operating temperature of 48 K is reached. Under pulsed excitation at duty cycles of 0.5%–1%, slightly higher (10%) peak powers are reached, and the device can be operated up to 67 K. Low threshold current densities of 165 and 185 A cm^{-2} are observed in pulsed and cw operation, respectively. The operation of the laser is examined using the Hakki–Paoli technique to estimate the net gain of the structure. © 2003 American Institute of Physics. [DOI: 10.1063/1.1559419]

Solid-state devices are nowadays extensively used to generate electromagnetic radiation with frequencies ranging from kilohertz up to petahertz. However, for the region from 1 to 10 THz, no compact and coherent sources are available, as electronics currently does not reach frequencies above 1 THz and laser diodes have not been able to operate at wavelengths longer than 30 μm (10 THz). The *p*-doped Ge laser¹ has for long time been the only semiconductor laser capable of emitting terahertz radiation, yet a device-like implementation appears to be unlikely in view of both technological and fundamental limitations. Quantum-cascade (QC) lasers,² on the other hand, soon after their demonstration at mid-infrared wavelengths, were considered to be promising candidates for a terahertz semiconductor laser. Several groups have reported electroluminescence from such structures,^{3–6} and finally terahertz QC lasers have been demonstrated.⁷ These latter devices emit several milliwatts peak power and operate up to 50 K heat sink temperature with low threshold current densities of 300 A cm^{-2} more recently, even lower threshold values of 200 A cm^{-2} have been obtained.⁸ Cw operation, a capability desired by many applications in astronomy, chemical sensing, and telecommunications, has been achieved very recently,^{9,10} thanks to improved fabrication and size reduction of the devices. Output powers up to a few hundred microwatts have been obtained.

In this letter, we report high-performance cw operation of a terahertz superlattice QC laser. A nominally identical replica of the original heterostructure of Ref. 7 was grown by molecular-beam epitaxy. Samples were processed by optical lithography and wet chemical etching into 150–180- μm -wide ridge stripes of depth 11.2 μm , exposing the bottom contact layer. Thermal evaporation of GeAu/Au (60 nm/60 nm) onto two 15 μm wide stripes on top of the ridges as well as on selective areas on the bottom contact layer (separated

by 25 μm from the laser ridges), followed by thermal annealing for 60 s at 420 °C under nitrogen atmosphere, provided ohmic contacts. The use of just two narrow stripes on the top reduces the waveguide losses, which are believed to be higher in annealed material, while the close side contacts reduce heating effects in the bottom layer. Evaporation of Cr/Au (10 nm/170 nm) covering both the bottom contact and the entire ridge allows for wire bonding (see inset of Fig. 1). The substrates were then thinned down to about 250 μm , their back was metallized with Cr/Au, and laser bars cleaved. The facets were left either untreated, or a high-reflection coating ($\text{Al}_2\text{O}_3/\text{Ti}/\text{Au}/\text{Al}_2\text{O}_3$) was deposited on the back facet. The devices were finally soldered onto copper blocks, wire-bonded, and mounted onto the cold finger of a continuous-flow cryostat. Light-current (*L–I*) characteristics under continuous excitation have been recorded by mounting a *f*/3.5 Winston cone with an exit diameter of 6 mm in front of one laser facet and using a calibrated pyroelectric radiometer. While the cone gathers all light from the facet, it still provides a divergent beam at the exit. This results in a collection efficiency much lower than unity (ideally 0.33 if the laser output were isotropic) for a detection element of area 1 cm^2 at a distance of 69 mm.

The measured power of a typical uncoated laser device is reported in Fig. 1 as a function of cw drive current. At low temperatures, we obtain almost 2.5 mW, with still more than 500 μW at 40 K. Lasing ceases at around a 45 K heat sink temperature. These values would translate into 7.5 and 1.5 mW, respectively, of total emitted power per facet, using the 0.33 collection efficiency. At 10 K, a low threshold current density of 210 A cm^{-2} is recorded. In the linear regime from threshold to 1 A, the slope efficiency, again corrected with the factor of 0.33, is 17 mW/A. This can be compared with the expected value

$$\frac{\partial P}{\partial I} = \frac{1}{2} N_P \frac{\alpha_M}{\alpha_M + \alpha_W} \frac{h\nu}{q_0} \tau, \quad (1)$$

^{a)}Electronic mail: koehler@nest.sns.it

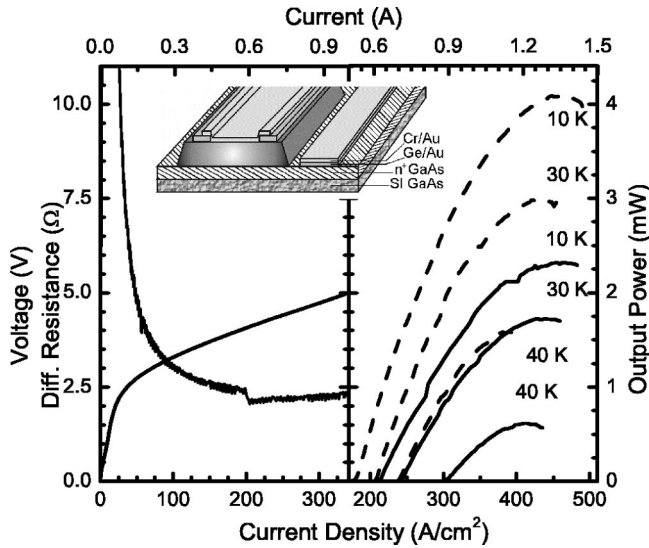


FIG. 1. L - I and V - I characteristics of 1.96-mm-long and 150- μ m-wide laser stripe, recorded in cw operation at different heat sink temperatures, are plotted in solid lines. The power values represent what was collected from one facet onto a calibrated pyroelectric detector after correction for the transmittance of the polyethylene window (0.63). The 7 K V - I characteristics and its derivative are shown in the left panel. Dashed lines represent data collected from a 2.23-mm-long device with a coated back-facet. Output powers are in this case more than 4 mW at 10 K and still 1.6 mW at 40 K. The maximum operating temperature increases only slightly to about 48 K. Due to the slightly different device size, the scale of the current refers only to the solid lines. The inset shows a schematic view of a processed laser stripe.

where P is the optical output power, I the injection current, α_M, α_W the outcoupling and waveguide loss, respectively, $h\nu$ the photon energy, $N_p = 104$ the number of periods, and q_0 the electronic charge. τ is a dimensionless constant that takes into account that, in QC lasers, the lower state population differs significantly from zero, and that the injection efficiency η_i of carriers into the upper laser state can deviate from unity. In a rate equation framework, τ can be derived to be^{11,12}

$$\tau = \left[1 - \frac{\tau_2}{\tau_3} \left(\frac{1}{\eta_i} - 1 \right) - \frac{\tau_2}{\tau_{32}} \right] \frac{\tau_3}{\tau_2 + \tau_3 [1 - (\tau_2/\tau_{32})]}, \quad (2)$$

where τ_3 , τ_2 are the total lifetimes of the upper and lower laser levels, respectively, and τ_{32} denotes the scattering time of electrons from level 3 to level 2. The presence of a considerable population in the lower laser level at threshold,¹³ indicated by the ratio of lifetimes τ_2/τ_{32} , is the main reason for the reduction of the slope efficiency from its ideal value. Inserting lifetimes calculated using Monte Carlo simulations,^{13,14} a slope efficiency of 55 mW/A can be computed, assuming a unity injection efficiency. The difference to the experimental value could be due to heating effects, uncertainties in the measurements, other scattering mechanisms not included in the simulations, and a nonunity injection efficiency. In Fig. 1, we also show the voltage and the differential resistance across the device as a function of the cw injected current. The voltage-current characteristic follows the well-known behavior of high resistance at low currents, and a turn-on towards lower differential resistance when the minibands align. The differential resistance shows the characteristic drop at threshold when the onset of stimulated emission reduces the lifetime τ_3 . Its clear visibility is

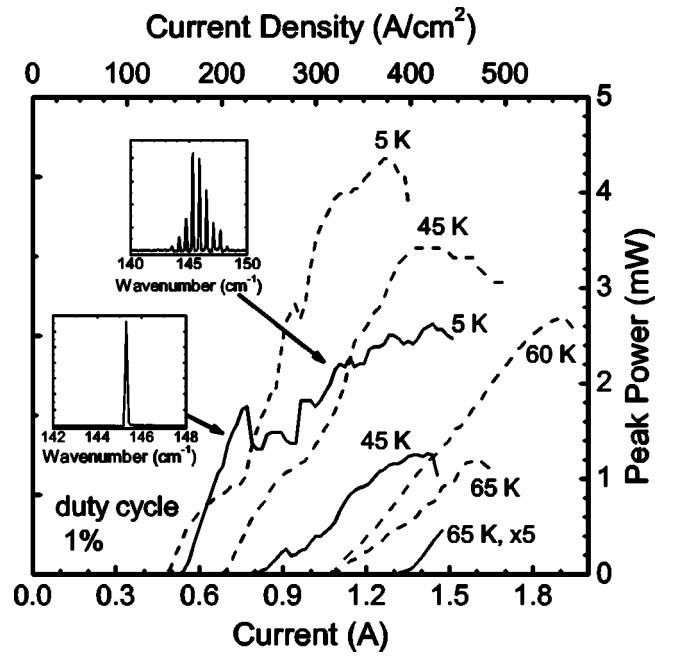


FIG. 2. L - I characteristics of the same device as in Fig. 1, recorded in pulsed operation at a duty cycle of 1% with a He-cooled Si bolometer. Dashed lines represent data collected from the device with a coated back-facet at a duty cycle of 0.5%. Due to the slightly different device size, the scale of the current density refers only to the solid lines.

in general a good indication of a high injection efficiency.¹¹ Substantial improvements in threshold current density, output power, and slope efficiency are obtained from a laser with its back facet covered with the high-reflection coating. Data recorded from this device are represented by the dashed lines in Fig. 1. A reduction of the threshold current density by about 10% (to 185 A cm⁻²) is achieved, and simultaneously the maximum output power increases to more than 4 mW.

For pulsed measurements, terahertz radiation was collected by an $f/1$ off-axis parabolic mirror, sent through a Fourier transform interferometer and focused again onto a liquid-He-cooled Si bolometer. The entire beam path was purged with purified air in order to minimize water vapor absorption. In Fig. 2, we show the L - I characteristics measured at a local duty cycle of 1%; that is, current pulses of 200-ns length were separated by 20 μ s. In order to calibrate the power reading at the bolometer, we first measured the average power of the device with the pyroelectric detector and found a value of 26 μ W, corresponding to 2.6 mW peak power. Since the preamplifier of the bolometer saturates at these power levels, we had to decrease the global duty cycle to obtain a reliable reading of the optical power. To this end, bursts of 200 pulses, each 200 ns long and separated by 20 μ s, were applied to the device at a repetition rate of 4 Hz, maintaining locally the duty cycle of the calibration measurements. This low repetition rate also provides sufficient cooling time for the detector element between two bursts. The output voltage of the bolometer was then monitored with an oscilloscope and read by a gated integrator. It was verified that increasing or decreasing the number of pulses did not affect the amplitude but only the length of the bolometer slow output pulse. Compared to cw operation, the threshold current density is reduced to 185 A cm⁻² at 5 K, which is a

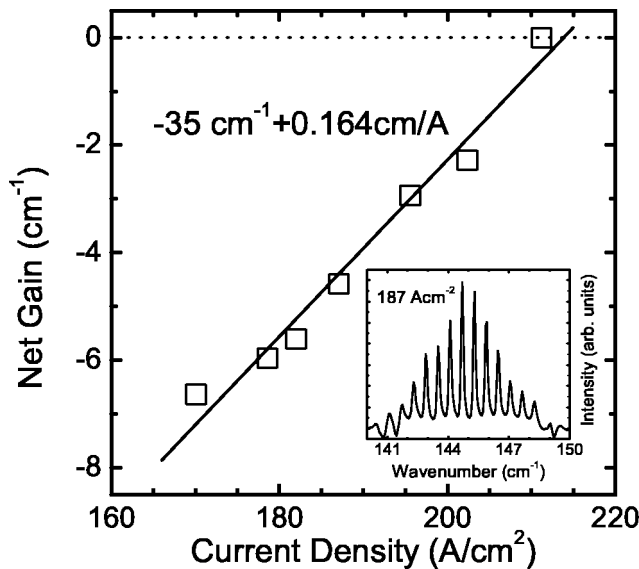


FIG. 3. Measurement of peak net gain as a function of injection current density at 8 K using the Hakki–Paoli technique; the dashed horizontal line indicates laser threshold. The slope of a linear fit to the data yields the gain constant. In the inset an example subthreshold spectrum is reported. Although the optical path was purged with purified air, some water-vapor absorption features are observable at 141 and 149 cm^{-1} ; as can be seen however, they do not affect the peak gain measurement at around 145 cm^{-1} .

very low value for a QC laser. This reduction is most likely due to the reduced heating of the device, which might lessen thermal backfilling and improve injection efficiency. This could also explain the higher slope efficiency of 25 mW/A observed in pulsed operation, a number much closer to the theoretical one. The decrease in optical output power between 0.8 and 1.0 A is reproducible and corresponds to the onset of multimode lasing (see inset of Fig. 2); a similar behavior, although less pronounced, is observed also in cw operation. Lasing is achieved up to a 67-K heat sink temperature with a 90- μW peak power at 65 K. The characteristics of the device with a coated back facet are shown as well. For this laser, output powers of about 4.5 mW are measured at 10 K with a reduction in threshold to 165 A cm^{-2} . More than 1 mW is emitted at 65 K.

We have then performed measurements of the net gain G as a function of continuous injection current density J following the technique pioneered by Hakki and Paoli.¹⁵ Subthreshold spectra from the 1.96-mm-long device of Fig. 1 were collected in rapid-scan mode with a resolution of 0.125 cm^{-1} averaging over 400 scans, and the net gain was extracted from the fringe contrast.¹⁵ The results obtained at 8 K are reported in Fig. 3. Close to threshold, the dependence appears to be reasonably linear, and a net modal gain $g\Gamma = 0.164 \text{ cm/A}$ is extracted. Unlike in mid-infrared QC lasers, where the transparency condition of the laser transition is readily reached close to zero injection current, in our structure the lower laser level is populated up to threshold and above.¹³ There is thus a minimum current density J_0 for which the transparency condition is reached. Therefore, an extrapolation of the data collected close to threshold to zero

current density cannot be used to extract the waveguide losses. In fact, such an interpolation would yield an unreasonably high value of 30 cm^{-1} , if corrected for the mirror losses of 5 cm^{-1} . For the same reason, the threshold gain, even assuming a linear behavior over the whole current range cannot be calculated as $g\Gamma J_{\text{th}}$. Nevertheless, in the linear part, the gain in the structure can be written as

$$G = g\Gamma(J - J_0) = \frac{4\pi z^2 q_0^2}{\epsilon_0 \lambda n L_p (2\gamma_{32})} (N_3 - N_2), \quad (3)$$

where N_3 , N_2 are the sheet densities in levels 3,2, $z = 7.8 \text{ nm}$ (the dipole matrix element between states 3 and 2), $\epsilon_0 = 8.85 \times 10^{-12} \text{ C/V m}$, $\lambda = 67 \mu\text{m}$, L_p is the length of one period, $n = 3.6$, and $2\gamma_{32} = 2 \text{ meV}$. This allows us to define an effective time τ_0 for the relaxation of population inversion, which can be extracted from the Hakki–Paoli analysis:

$$\tau_0 = q_0 \frac{\partial G}{\partial J} \bigg/ \frac{\partial G}{\partial (N_3 - N_2)}. \quad (4)$$

We obtain a value of 0.96 ps, which is in fair agreement with previous Monte Carlo simulations.¹³

This work was supported in part by the European Commission through an IST Framework V FET project WANTED. Two of the authors (R.K.) and (A.T.) acknowledge support by the C.N.R. and the Fondazione Cassa di Risparmio di Pisa; two others (E.H.L.) and (A.G.D.) acknowledge support from Toshiba Research Europe Ltd. and the Royal Society, respectively. The authors would like to thank J. Faist for communicating his results prior to publication.

- ¹A. A. Andronov, I. V. Zverev, V. A. Kozlov, Yu N. Nozdrin, S. A. Pavlov, and V. N. Shastin, *JETP Lett.* **40**, 804 (1984).
- ²J. Faist, F. Capasso, D. L. Sivco, C. Sirtori, A. L. Hutchinson, and A. Y. Cho, *Science* **264**, 553 (1994).
- ³M. Rochat, J. Faist, M. Beck, U. Oesterle, and M. Illegems, *Appl. Phys. Lett.* **73**, 3724 (1998).
- ⁴B. S. Williams, B. Xu, Q. Hu, and M. R. Melloch, *Appl. Phys. Lett.* **75**, 2927 (1998).
- ⁵J. Ulrich, R. Zobl, K. Unterrainer, G. Strasser, and E. Gornik, *Appl. Phys. Lett.* **76**, 19 (2000).
- ⁶R. Köhler, A. Tredicucci, F. Beltram, H. E. Beere, E. H. Linfield, A. G. Davies, and D. A. Ritchie, *Appl. Phys. Lett.* **80**, 1867 (2002).
- ⁷R. Köhler, A. Tredicucci, F. Beltram, H. E. Beere, E. H. Linfield, A. G. Davies, D. A. Ritchie, R. C. Iotti, and F. Rossi, *Nature (London)* **417**, 156 (2002).
- ⁸M. Rochat, L. Ajili, H. Willenberg, J. Faist, H. Beere, G. Davies, E. Linfield, and D. Ritchie, *Appl. Phys. Lett.* **81**, 1381 (2002).
- ⁹L. Ajili, G. Scalari, D. Hofstetter, M. Beck, J. Faist, H. Beere, G. Davies, E. Linfield, and D. Ritchie, *Electron. Lett.* **38**, 1675 (2002).
- ¹⁰S. Barbieri, J. Alton, M. Evans, S. S. Dhillon, H. E. Beere, E. H. Linfield, A. G. Davies, D. A. Ritchie, R. Köhler, A. Tredicucci, and F. Beltram, *IEEE J. Quantum Electron.* (in press).
- ¹¹C. Sirtori, F. Capasso, J. Faist, A. L. Hutchinson, D. L. Sivco, and A. Y. Cho, *IEEE J. Quantum Electron.* **34**, 1722 (1998).
- ¹²V. B. Gorfinkel, S. Luryi, and B. Gelmont, *IEEE J. Quantum Electron.* **32**, 1995 (1996).
- ¹³R. Köhler, R. C. Iotti, A. Tredicucci, and F. Rossi, *Appl. Phys. Lett.* **79**, 3920 (2001).
- ¹⁴D. Indjin, P. Harrison, R. W. Kelsall, Z. Ikonic, *THz 2002 Conference Proceedings*, IEEE Cat. No. 02EX621, 2002, p. 97.
- ¹⁵B. W. Hakki and T. L. Paoli, *J. Appl. Phys.* **46**, 1299 (1975).